

## Theory of conformational transitions of viral shells

Thomas Guérin

*Ecole Polytechnique, 91128 Palaiseau, France*

Robijn Bruinsma

*Department of Physics and Astronomy, University of California, Los Angeles, California 90025, USA*

(Received 23 March 2007; published 19 December 2007)

We propose a continuum theory for the conformational transitions of viral shells. Conformational transitions of viral shells, as encountered during viral maturation, are associated with a *soft mode instability* of the capsid proteins [F. Tama and C. L. Brooks, *J. Mol. Biol.* **345**(2), 299 (2005)]. The continuum theory presented here is an adaptation of the Ginzburg-Landau theory of soft-mode structural phase transitions of solids to viral shells. The theory predicts that the conformational transitions are characterized by a pronounced softening of the shell elasticity in the critical region. We demonstrate that the thermodynamics of the conformational transition can be probed quantitatively by a micromechanical atomic force microscope study. The external force can drive a capsid into a state of *phase coexistence* characterized by a highly nonlinear force deformation curve.

DOI: [10.1103/PhysRevE.76.061911](https://doi.org/10.1103/PhysRevE.76.061911)

PACS number(s): 87.15.La, 46.32.+x, 87.17.Aa, 87.64.Dz

### I. INTRODUCTION

The icosahedral protein shells that surround the genome of spherical viruses resemble curved, two-dimensional (2D) crystals. Caspar and Klug (CK) [1] showed that the location of the proteins on a viral shell can be classified by the methods of crystallography. The similarity between viral shells and 2D solids has been further extended to include concepts such as elastic *stress* and *strain*, normally reserved for bulk materials. The continuum elasticity theory of thin shells appears capable of accounting not only for the global shape of large icosahedral and nonicosahedral viruses [2] but also for the response of viral shells to applied mechanical force, produced for instance by an atomic force microscope (AFM) [3]. Even the structural failure of viral shells under applied force appears to follow the predictions of elasticity theory [4].

One aim of this paper is to investigate whether methods of *solid-state physics* can be applied to viral shells also, specifically to the *conformational changes* of capsid proteins that take place during viral maturation [5]. Maturation refers to the postassembly, irreversible, exothermic reorganization of a precursor “procapsid.” This reorganization may follow an autocatalytic cleavage reaction of capsid polyproteins into multiple parts, as takes place for instance during the maturation of the Picornaviruses or the Lentiviruses [6]. Protein conformational changes also may initiate the release of the viral genome, as in the case of the FHV (Flock House virus) [7]. Conformational changes need not be associated with a chemical reaction but also can be triggered by changes in salt concentration or *pH*, as in the case of CCMV (Cowpea chlorotic mottle virus) [8].

Capsid protein conformational changes are inherently *cooperative* because the proteins are closely locked together as part of the shell. If only *some* of the capsid proteins of a viral shell would undergo a conformational change and/or chemical reaction then this would violate the CK “quasiequivalent” arrangement. The fact that the CK arrangement describes the structure of so many different viral shells indicates that vio-

lations of the CK arrangement involve a significant free energy penalty. In 1980, Caspar proposed the concept of *allosteric coupling* [9–11] stating that the conformational change of one capsid protein—produced, say, by a chemical reaction—triggers secondary conformational changes in neighboring proteins, which then—in opposition to Le Chatelier’s principle—shift the chemical equilibrium of the neighboring proteins to favor the reaction or conformational change.

Similar cooperative conformational changes occur in solid-state materials, such as ferroelectrics, martensites, and solid alloys, in the form of collective, atomic-level rearrangements of the basic unit cell, known as *structural phase transitions* [12]. Rearrangement of a single unit cell influences not only adjacent unit cells but also distant regions of the material through long-range elastic strains. A characteristic of structural phase transitions is the development of a *soft mode*, associated with an unusually slow phonon mode. Soft modes are accompanied by anomalous elastic behavior. Interestingly, all-atom numerical studies by Tama and Brooks of conformational transitions of viral shells report that the conformational changes of the shell follow the trajectory of the lowest, nondegenerate mode of the shell and that this mode can soften in the presence of  $\text{Ca}^{++}$  ions [13,14]. This paper is based on the premise that the conformational changes of allosterically coupled viral shells and the structural phase transitions of solids are in essence the same phenomenon. An effective theoretical description of soft-mode structural phase transitions of solids is available in the form of the Ginzburg-Landau (GL) theory [15] and we will adapt this method to describe conformational transitions of viral shells. It is, incidentally, important to distinguish soft modes of this type, driven by internal conformational changes of the proteins, (“type I”), from the soft mode that recently was shown [16] to characterize elastic shells with icosahedral symmetry (“type II”). A type-II soft mode could appear only if capsid radii are close to the *buckling transition*, where the shape of the shell changes from spherical to

polyhedral, while a type-I soft mode could take place for arbitrary values of the capsid radius.

The thermodynamics of structural phase transitions of solids has been extensively studied but, so far at least, the thermodynamics of conformational transitions of viral shells have not yet been probed on a quantitative basis. We will show that the micromechanical deformation of a viral shell by osmotic pressure or an AFM could be used to probe, on a quantitative basis, the thermodynamics of conformational changes. Specifically, the free energy difference per unit area and the interfacial energy could be obtained from an AFM study if the results are analyzed by the methods presented in this paper. An important prediction of the formalism is that viral conformational changes can produce softening of the *stretching stiffness* of the shell.

The organization of the paper is as follows. In Sec. II, we will construct a continuum free energy for spherical viral shells that can undergo a cooperative conformational change and/or chemical reaction, including both the short-range and long-range cooperativity and we will analyze the thermodynamics for uniform shells. In Sec. III we use this free energy to compute the response of the shell to an external force and show that the application of an external force can produce *two-phase coexistence* provided the shell in its initial state is stiffer than in the final state. In the concluding section we apply the concepts developed in this paper to two specific viral shells (CCMV and HK97 (Hong Kong 97)).

## II. CAPSID FREE ENERGY

The continuum free energy of a viral shell with internal degrees of freedom will be written as the sum of a Gibbs free energy for a *reaction coordinate* describing the internal conformational change of the constituent proteins plus an elastic strain energy that describes longer-range cooperative interactions between the proteins. Starting with the first part, the conformational change of the capsid proteins is described by a reaction coordinate  $\eta$  that links two states of the protein: the “initial state”  $\eta=0$ , which could describe the conformation of the proteins of an immature capsid, and the “final state”  $\eta=\eta_+$ , which could describe the conformation of a mature capsid protein. This reaction coordinate should *not* be viewed here as an atomic-level displacement—as it is for conformational phase transitions in bulk solids—but rather as the amplitude of a *collective degree of freedom* of the capsid proteins that follows a steepest-descent trajectory across the lowest activation energy barrier separating the initial and final states. As mentioned, Tama and Brooks [14] report that the conformational change of a viral shell can be described by the amplitude of the lowest, nondegenerate normal mode of the capsid protein. The reaction coordinate  $\eta$  is to be identified with this dominant Tama-Brooks normal mode.

The Gibbs free energy of the reaction  $g_0(\eta)$  is a function of this reaction coordinate with, in general, minima at the initial and final state values of  $\eta$  separated by one or more maxima. We will assume here the simple case of just a single maximum, the *transition state* (see Fig. 1). Because we are describing a 2D *layer* of proteins,  $g_0(\eta)$  is the Gibbs free

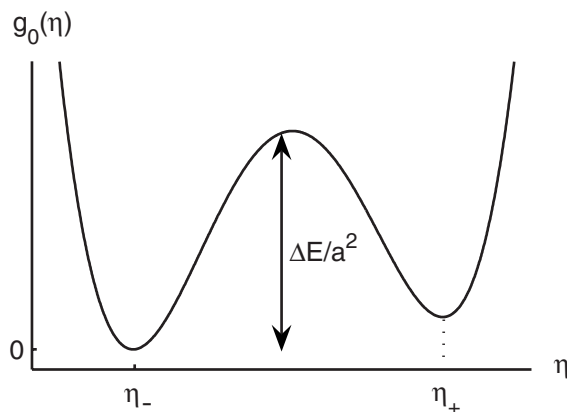


FIG. 1. Schematic Gibbs free energy  $g_0(\eta)$  per unit area for the maturation reaction as a function of the reaction coordinate  $\eta$ . The first minimum  $\eta_-$ , near  $\eta=0$ , corresponds to the initial state and the second minimum,  $\eta_+$ , to the final state. The free energy barrier per unit area separating the two minima equals  $\Delta E/a^2$ .

energy *per unit area* of capsid. The total Gibbs free energy for the reaction is thus the difference  $g_0(\eta^+) - g_0(0)$  times the capsid area. Since—typically—activation energy barriers for the conformational change of a protein are in the range of  $10 k_B T$ , the free energy barrier per protein  $\Delta E/a^2$  separating the two minima of  $g_0(\eta)$  is expected to be of the order of  $10 k_B T$  per  $\text{nm}^2$ .

During the transformation reaction, the capsid need not be in a uniform state, so we must allow the reaction coordinate  $\eta(\vec{x})$  to depend on the location  $\vec{x}$  on the capsid shell. The simplest free energy for a position-dependent reaction coordinate has the form

$$H_{int} = \int dS \left( \frac{\Gamma}{2} (\vec{\nabla} \eta)^2 + g_0(\eta) \right), \quad (1)$$

where the integral in Eq. (1) extends over the surface of the capsid. The square-gradient term of Eq. (1) describes *short-range* cooperativity between neighboring proteins. This term is minimized if adjacent proteins have the same value of the reaction coordinate. The parameter  $\Gamma$  determines the “healing length”  $\xi = \sqrt{\Gamma/g_0''}$  with  $g_0''$  the *curvature* of the reaction coordinate free energy. This healing length is the characteristic length scale for spatial changes of the reaction coordinate. We can estimate  $\xi$  as  $a(\delta E/\Delta E)^{1/2}$ , with  $\delta E$  the typical cohesive binding free energy of capsid proteins, which is of the order of  $10 k_B T$  according to thermodynamics studies of capsid assembly [17].

Next, we turn to the *strain energy* that describes the center-of-mass displacements of the capsid proteins away from a strain-free reference state in response to changes of the reaction coordinate or due to an externally applied force. As our strain-free “reference state,” we will take a uniform sphere of radius  $R$  with the reaction coordinate equal to zero (strain heterogeneity associated with the twelve fivefold sites of viral shells is not included in the present paper). We then define deformations of the reference state by the two functions  $f(\vec{r})$ , the displacement along the (outward) radial direction and  $\vec{u}(\vec{r})$ , the displacement in a plane tangent to the

sphere. According to the theory of thin elastic shells, the elastic free energy cost associated with these displacements is given by

$$H_E = \int dS \left( \frac{\kappa}{2} \left[ \Delta f + \frac{2f}{R^2} \right]^2 + \frac{K}{2} u_{ii}^2 + \mu \left( u_{ij} - \frac{1}{2} u_{ll} \delta_{ij} \right)^2 \right) \quad (2)$$

The integral again extends over the surface of the reference sphere. The first term is the “out-of-plane” bending energy, with  $\Delta$  the Laplacian. The quantity in square brackets is the total *deviation* of the mean curvature away from the mean curvature  $2/R$  of the strain-free reference state with  $2f/R^2$  the change in mean curvature for uniform expansion or contraction of the shell [18]. Micromechanical studies indicate that the bending modulus  $\kappa$ , which has units of energy, lies in the range of 10–100  $k_B T$  [4]. In the second term, the “in-plane” elastic energy,  $u_{ij}$  is the strain tensor defined by

$$u_{ij} = \frac{1}{2} \left( \frac{\partial u_i}{\partial x_j} + \frac{\partial u_j}{\partial x_i} \right) + \frac{1}{2} \frac{\partial f}{\partial x_i} \frac{\partial f}{\partial x_j} + \delta_{ij} \frac{f}{R}. \quad (3)$$

The first term is the conventional strain tensor of a flat sheet. The second—nonlinear—term can be understood by considering the stretching strain produced by *tilting* a surface area element at fixed projected area. The last term describes the area change  $\Delta A/A$  produced by uniform radial swelling or contraction of the sphere.  $K$  and  $\mu$  are here, respectively, the (two-dimensional) area modulus and shear modulus of the shell. These moduli have not been independently measured. However, the *buckling length*  $l_B = \sqrt{\kappa/Y}$ , with  $Y = 4K\mu/(K + \mu)$  the two-dimensional *Young's modulus*, can be estimated from structural studies and is in the range of a nanometer (we will in the following assume that the viral shell radius  $R$  is large compared to this buckling length), while micromechanical studies [4] indicate that  $Y$  is of the order of  $10^2 k_B T/\text{nm}^2$  and  $\kappa$  of the order of  $10^2 k_B T$ .

The coupling between the reaction coordinate and the elastic strain tensor will be inferred from symmetry considerations following the GL method. If the initial and final states of the capsid have the same symmetry (as is the case for conformational transitions of viral shells) then the reaction coordinate  $\eta$  has to transform as a *scalar* under the symmetry operations of the reference state. The lowest-order scalar combining the reaction coordinate and the strain tensor is the product  $\eta u_{ii}$  of  $\eta$  with the trace of the strain tensor. Physically, this term describes the swelling or contraction of the capsid in response to the reaction in the form of a coupling of  $\eta$  to a specific linear combination of the in-plane and out-of-plane displacements [see Eq. (3)]. Our final expression for the continuum free energy of a capsid whose proteins have an internal scalar degree of freedom is then

$$\mathcal{F} = \int dS \left( \frac{\kappa}{2} \left( \Delta f + \frac{2f}{R^2} \right)^2 + \frac{K}{2} u_{ii}^2 + \mu \left( u_{ij} - \frac{1}{2} u_{ll} \delta_{ij} \right)^2 + \frac{\Gamma}{2} (\vec{\nabla} \eta)^2 + g_0(\eta) - \gamma_0 \eta u_{ii} \right) \quad (4)$$

with  $\gamma_0$  a constant. If the constant is positive, then the conformational change produces swelling of the shell and contraction if the constant is negative. If the viral shell also is

filled with one or more genome molecules then we must include the effect of the *osmotic pressure*  $\Pi_0$  exerted on the (semipermeable) capsid wall. For bacteriophage viruses  $\Pi_0$  has been measured to be in the range of ten's of atmospheres [19]. Osmotic pressure can be included in Eq. (4) by adding the term

$$W = - \int dS \Pi_0 f, \quad (5)$$

representing the work by the osmotic pressure as we change the enclosed volume.

As a first step in analyzing Eq. (4), we note that the *stress tensor* of the shell, defined as  $\sigma_{ij} = \delta F / \delta u_{ij}$ , is given by

$$\sigma_{ij} = K u_{ll} \delta_{ij} + 2\mu \left( u_{ij} - \frac{1}{2} u_{ll} \delta_{ij} \right) - \gamma_0 \eta \delta_{ij}. \quad (6)$$

The stress tensor depends explicitly on the conformational state of the proteins, unlike the strain tensor. Next, if we minimize Eq. (4) with respect to both the reaction coordinate and the strain tensor, one obtains after a tedious calculation the following set of coupled equations:

$$\kappa \left( \Delta^2 f + \frac{4\Delta f}{R^2} + \frac{4f}{R^4} \right) - \vec{\nabla} \cdot (\vec{\sigma} \cdot \vec{\nabla}) f + \frac{1}{R} \text{Tr} \vec{\sigma} = \Pi_0, \quad (7)$$

$$\vec{\nabla} \cdot \vec{\sigma} = 0, \quad (8)$$

$$-\Gamma \Delta \eta + \frac{dg_0}{d\eta} - \gamma_0 \text{Tr} \vec{u} = 0. \quad (9)$$

The first two equations represent a variant of the challenging nonlinear Föppl–von Karmán equations for thin elastic shells. Equation (9) shows that if the trace of the strain tensor is nonzero then the reaction coordinate is forced out of the equilibrium states shown in Fig. 1. In addition, the dependence of the stress tensor on the reaction coordinate as given by Eq. (6) provides a second coupling between the elastic and internal degrees of freedom.

If no external force is applied to the shell, then we should look for *uniform* solutions of these equations. In that case, the equations simplify to

$$4 \left( \frac{\kappa}{R^2} + K \right) \frac{f}{R^2} - \frac{2\gamma_0}{R} \eta = \Pi_0, \quad (10)$$

$$\frac{dg_0}{d\eta} - \frac{2\gamma_0 f}{R} = 0, \quad (11)$$

$$\sigma_{ij} = \frac{\Pi_0 R}{2} \delta_{ij}. \quad (12)$$

Equation (12) relates the trace of the stress tensor to the pressure difference across the shell. If we interpret this trace as the *tension* along the surface of the shell, then Eq. (12) simply reduces to Laplace's law relating tension to pressure for a spherical vessel. Next, Eq. (10) provides a linear relation between the radial swelling of the capsid and the internal osmotic pressure. If—as we are assuming— $R$  is large compared to the buckling length, then the 2D stretching

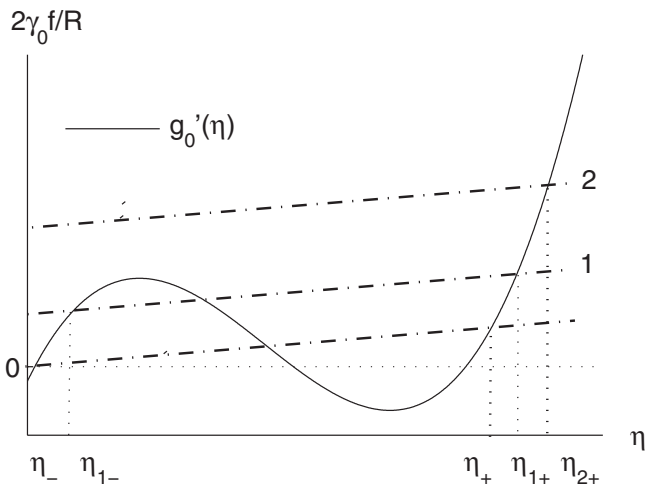


FIG. 2. Graphical construction for obtaining equilibrium values of the reaction coordinate. The solid line shows  $dg_0/d\eta$ . Intercepts of  $dg_0/d\eta$  with a straight line (dashed) represent possible values for the reaction coordinates. Only intercepts with  $d^2g_0/d\eta^2$  positive can represent thermodynamically stable states. Intercepts with the straight line through the origin correspond to the case of zero osmotic pressure. If the pressure increases (lines labeled 1 and 2) then the solution corresponding to the initial state disappears above a threshold “spinodal” pressure.

modulus  $K$  will determine the proportionality constant. By the graphical construction of Fig. 2, possible solutions can be obtained for the equations.

The intercepts of  $dg_0/d\eta$  with the horizontal axis represent the possible values for the reaction coordinate in the absence of coupling to strain. The intercepts of  $dg_0/d\eta$  with the straight line passing through the origin represent the case of finite strain coupling, but zero osmotic pressure. If there are three intercepts, then the intercept with the smallest value of  $\eta$  corresponds to the immature state while the intercept with the largest value of  $\eta$  corresponds to the mature state. In general, only intercepts with positive slope for  $dg_0/d\eta$ , i.e., with  $d^2g_0/d\eta^2 > 0$ , are admissible as thermodynamically stable states (we will show below that full thermodynamic stability imposes a more stringent condition). Intersections of  $dg_0/d\eta$  with the other two straight lines (labeled 1 and 2) show possible solutions for increasing values of the osmotic pressure. As the pressure increases, the  $\eta$  values of both the mature and immature states ( $\eta_{1-}$ , respectively,  $\eta_{1+}$ ) shift upward. A structural transition requires the crossing of an intervening free energy barrier. The unstable free energy maximum, or transition state, separating the two states corresponds here to the second intercept, with negative  $d^2g_0/d\eta^2$ . At a critical pressure, the immature solution fuses with this unstable state. At higher pressures, the capsid can only be in the mature state. In the theory of phase transitions, this phenomenon is known as a “spinodal” instability.

The radial displacement in the two competing states is generally related to the reaction coordinate by

$$f_{\pm} \cong \frac{R^2}{4K} \left( \Pi_0 + \frac{2\gamma_0}{R} \eta_{\pm} \right). \quad (13)$$

The free energy per unit area as a function of the reaction coordinate only is given by

$$(\mathcal{F} + W)/4\pi R^2 = \left( g_0(\eta) - \frac{\gamma_0^2}{2K} \eta^2 - \frac{\Pi_0 \gamma_0 R}{2K} \eta - \frac{\Pi_0^2 R^2}{8K} \right). \quad (14)$$

According to Eq. (14), pressure provides a bias towards the mature state assuming the coupling parameter  $\gamma_0$  to be positive. Note, from Eq. (14), that the coupling between the strain and reaction coordinates *always* has a destabilizing effect on the immature state, irrespective of the sign of the coupling constant. Thermodynamic stability requires the second derivative of the right-hand side of Eq. (14) to be positive, which is the case as long as  $d^2g_0/d\eta^2 > \gamma_0^2/K$ .

This discussion was identical to that of a classical *first-order phase transition*. This suggests that—at least near the transition point—it might be possible to encounter “phase coexistence” states where the capsid is partly in the immature contracted state and partly in the mature swollen state with the two states separated by a *phase boundary* that divides the capsid in two sections. To develop this analogy explicitly, assume that the reaction coordinate rapidly varies between the two minima of the free energy across this phase boundary while the radial displacement remains constant. It then follows, from Eq. (11), that we must demand the slope  $dg_0/d\eta$  to be the same on opposite sides of the boundary,

$$\frac{dg_0}{d\eta_-} \approx \frac{dg_0}{d\eta_+}, \quad (15)$$

where we approximated the values of the order parameter on opposite sides of the boundary with the two free energy minima. Integration of Eq. (11) across the boundary gives

$$g_0(\eta_+) - g_0(\eta_-) \approx \frac{2\gamma_0 f_b}{R} (\eta_+ - \eta_-). \quad (16)$$

Here,  $f_b$  is the value of the radial displacement at the phase boundary. Equations (15) and (16) have the familiar form of the phase-coexistence conditions for a first-order phase transition, such as, for example, for a liquid-gas boundary in the presence of applied pressure. In that case,  $f_b$  would play the role of pressure and  $\eta$  that of density. We can solve Eqs. (15) and (16) by applying the usual Maxwell equal-area construction as shown in Fig. 3.

It follows from the Maxwell construction that phase coexistence indeed *is* possible but only for a very particular value  $f_b$  for the radial swelling, just as liquid-gas phase coexistence at a certain temperature is possible only for a particular value of the pressure.

Unlike the pressure of a liquid-gas system, the radial displacement of the present problem is *not* an external thermodynamic parameter and must be determined from a solution of Eqs. (7)–(9). However, the radial displacement could be changed by the application of an external force. This suggests that the study of a capsid shell that is subject to conformational changes by micromechanical methods should be very interesting. Specifically, it would be very striking if we could drive viral shells into a state of phase coexistence under the application of an external force probe. This requires however a study of the solutions of Eqs. (7)–(9) for a de-

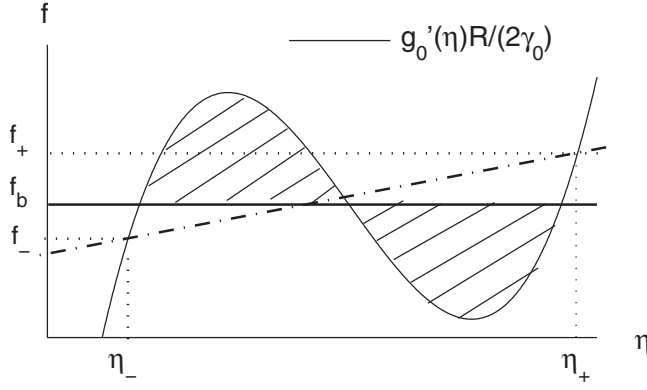


FIG. 3. Maxwell equal-area construction determining the radial displacement  $f_b$  for which initial and final states can coexist. The horizontal axis is the reaction coordinate  $\eta$ . The vertical axis is the radial displacement  $f$ , with  $\gamma$  the coupling constant between reaction coordinate and radial displacement. Radial displacements and reaction coordinates corresponding to the initial and final states are indicated. The dashed line shows the relation between reaction coordinate and displacement.

formed inhomogeneous capsid in the presence of an external force, which we will do in the next section.

### III. NONUNIFORM CAPSIDS

In this section we examine solutions of Eqs. (7)–(9) when both the radial displacement and the order parameter are allowed to vary with position. We will focus on the specific case of a capsid that is close to the transition point between the swollen and contracted states. The capsid is exposed to an external point force, of magnitude  $F$ , exerted along the radial direction (see Fig. 4). The force produces a radially symmetric dimple with indentation profile  $f(r)$  and reaction coordinate profile  $\eta(r)$  with  $r$  the arc distance from the point of force application along the capsid surface. Actual micro-mechanical probes, such as an AFM, are of course not very well described as point forces. Numerical studies show however that if the applied force is weak, then a point force gives the same scaling relation for the force-displacement relation as the force applied by a more realistic hemispherical surface [4].

Let  $\delta$  be the lateral size of the dimple produced by the point force (see Fig. 4). In Eq. (3), the last (linear) term of

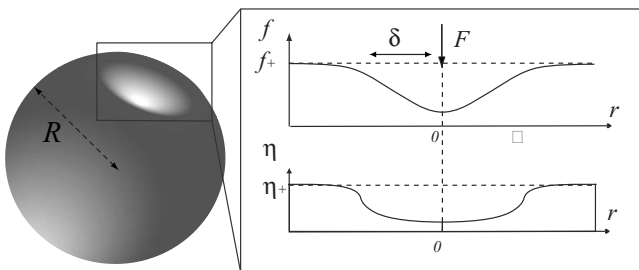


FIG. 4. Indentation profiles  $f(r)$  and  $\eta(r)$  of a capsid subject to an applied point force  $F$ . The capsid is resting on a surface. The dimple has a force-independent width  $\delta \sim (Rl_B)^{1/2}$  with  $R$  the radius and  $l_B$  the buckling length.

the strain tensor will dominate over the second (nonlinear) term as long as  $f \ll \delta^2/R$ . If one neglects the nonlinear term and compares the stretching and bending energies in the free energy equation (4), one finds that the dimple size must be of the order of  $\delta \sim (Rl_B)^{1/2}$  with  $l_B = \sqrt{\kappa/Y}$  the buckling length (recall that  $Y$  is the 2D Young's modulus). This dimple size is thus independent of the applied force and small compared to the radius of the capsid since by assumption  $R$  is large compared to the buckling length  $l_B$ . The condition  $f \ll \delta^2/R$  allowing neglect of the nonlinearity in the strain tensor is satisfied as long as the indentation  $f$  is small compared to the buckling radius  $l_B$ . The mathematical analysis greatly simplifies in that case. We can assume that the spatial variation of  $f$ ,  $\eta$ , and  $\vec{u}$  is restricted to a dimple region that is small compared to the radius of the sphere, while outside the dimple region, both  $f$  and  $\eta$  reduce to their appropriate limits  $\eta_{\pm}$  and  $f_{\pm}$  corresponding to the uniform state, as discussed in the previous section. Note that, even though the elasticity equations can be linearized under these conditions, Eq. (9) for the reaction coordinate still remains nonlinear.

The nonzero components of the linearized stress tensor [see Eq. (6)] are given by

$$\begin{aligned} \sigma_{rr} &= \sigma_0 + K \left( \vec{\nabla} \cdot \vec{u} + \frac{2(f-f_{\pm})}{R} \right) - \gamma_0(\eta - \eta_{\pm}) + \mu \left( \frac{du_r}{dr} - \frac{u}{r} \right), \\ \sigma_{\theta\theta} &= \sigma_0 + K \left( \vec{\nabla} \cdot \vec{u} + \frac{2(f-f_{\pm})}{R} \right) - \gamma_0(\eta - \eta_{\pm}) - \mu \left( \frac{du_r}{dr} - \frac{u}{r} \right), \\ \sigma_{r\theta} &= 0, \end{aligned} \quad (17)$$

with  $\sigma_0 = \Pi_0 R/2$  being the tension of the shell produced by the osmotic pressure. The condition that  $\vec{\nabla} \cdot \vec{\sigma} = 0$  translates into a relation between the in-plane displacement, the out-of-plane displacement, and the reaction coordinate,

$$(K + \mu) \vec{\nabla} \cdot \vec{u} + \frac{2K}{R} f - \gamma_0 \eta = \sigma_0. \quad (18)$$

It will be convenient in the following to redefine  $f$  and  $\eta$  by subtracting off the uniform state solution. In terms of the redefined variables, the in-plane displacement can be eliminated using Eq. (18) with the result

$$\kappa \Delta^2 f - \sigma_0 \Delta f + \frac{Y}{R^2} f - \frac{2\gamma}{R} \eta \cong -F \delta(\vec{r}), \quad (19)$$

$$-\Gamma \Delta \eta + \frac{dg}{d\eta} - \frac{2\gamma}{R} f = 0. \quad (20)$$

Both the coupling coefficient  $\gamma$  and the reaction free energy have been redefined here as well:  $\gamma = \gamma_0 \mu / (\mu + K)$  and  $g(\eta) = g_0(\eta) - \gamma_0^2 \eta^2 / [2(K + \mu)]$ . Note that the pressure-induced tension of the shell plays the role of a *surface energy*. The in-plane displacement field can be eliminated from the free energy as well,

$$\mathcal{F} = \int dS \left( \frac{\kappa}{2} (\Delta f)^2 + \frac{\sigma_0}{2} (\vec{\nabla} f)^2 + \frac{Y}{2R^2} f^2 + g(\eta) + \frac{\Gamma}{2} (\vec{\nabla} \eta)^2 - \frac{2\gamma}{R} \eta f + F \delta(\vec{r}) f \right), \quad (21)$$

which will form the basis for calculations of the indentation profiles.

### A. Linear response regime

In the linear response regime, the applied force is so weak that the reaction coordinate remains close to the minimum of the reaction free energy of the uniform state. In that case, we can expand the reaction free energy to second order around the appropriate minimum. Inserting this in Eq. (19), we encounter again the characteristic healing length  $\xi_{\pm} = \sqrt{\Gamma/g''(\eta_{\pm})}$  for the spatial variation of the reaction coordinate. After taking the Laplacian of Eq. (19), we can use Eqs. (19) and (20) to eliminate the reaction coordinate from Eq. (19) with the result

$$\begin{aligned} \kappa \Delta^2 f - \sigma_0 \Delta f + \frac{Y_{eff}}{R^2} f + F \delta(\vec{r}) \\ = \xi^2 \Delta \left( \kappa \Delta^2 f - \sigma_0 \Delta f + \frac{Y}{R^2} f + F \delta(\vec{r}) \right). \end{aligned} \quad (22)$$

Here,

$$Y_{eff} = Y - \frac{4\gamma^2}{g''(\eta_{\pm})} \quad (23)$$

represents an *effective* Young's modulus that is always smaller than the bare Young's modulus. We will discuss Eq. (22) separately for the two regimes  $R \gg \xi^2/l_B$  and  $R \ll \xi^2/l_B$ .

#### 1. $R \gg \xi^2/l_B$

For large capsids with  $R \gg \xi^2/l_B$ , the healing length  $\xi$  of the reaction coordinate is small compared to the dimple size  $\delta \sim (Rl_B)^{1/2}$ . In that regime, the reaction coordinate can “follow” spatial variations of the radial displacement, which means that we can drop the right-hand side of Eq. (22),

$$\kappa \Delta^2 f - \sigma_0 \Delta f + \frac{Y_{eff}}{R^2} f \approx -F \delta(\vec{r}). \quad (24)$$

Equation (24) for the indentation profile has the same form as one for a spherical elastic shell without internal degrees of freedom provided the bare Young's modulus is replaced by Eq. (23). The radially symmetric solution of Eq. (24) with the appropriate boundary conditions at infinity is

$$\frac{f(r)}{R} = \left( \frac{F}{2\pi\sqrt{Y_{eff}\kappa}} \right) \frac{1}{\sin(2\theta)} \text{Im} K_0 \left( \frac{r}{\delta} e^{i\theta} \right). \quad (25)$$

Here  $K_0(z)$  is a modified Bessel function of the second kind with complex argument while  $\delta = \sqrt[4]{R^2 \kappa / Y_{eff}}$  is the effective dimple radius. The complex number  $(1/\delta)e^{i\theta}$  is here a root of  $\kappa X^4 + \sigma_0 X^2 + Y/R^2$ , the characteristic polynomial of Eq. (24) [20]. The phase angle  $\theta = 1/2 \arccos(\Pi_0/\Pi_g)$  is a function of

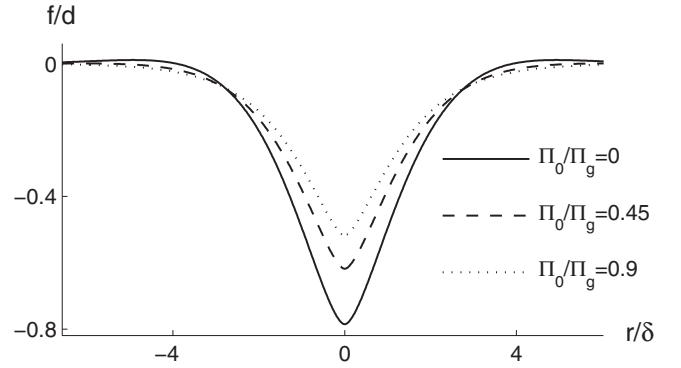


FIG. 5. Dimple profile in the linear response regime for large capsids ( $R \gg \xi^2/l_B$ ). The horizontal axis is the distance  $r$  from the probe in units of the characteristic in-plane width  $\delta = \sqrt[4]{R^2 \kappa / Y_{eff}}$  of the dimple. The vertical axis is the out-of-plane displacement  $f$  in units of  $d = \left( \frac{FR}{2\pi\sqrt{Y_{eff}\kappa}} \right)$ , the characteristic size of the depth of the dimple. The dimensionless pressure osmotic pressure  $\Pi/\Pi_g$ , with  $\Pi_g = 4\sqrt{\kappa Y_{eff}}/R^2$ , ranges from 0 to 1.8.

the internal pressure expressed in dimensionless units of a gauge pressure  $\Pi_g = 4\sqrt{Y_{eff}\kappa}/R^2$  (in the range of  $10^2$  atm). The force-deformation relation is linear,

$$\frac{|f(r=0)|}{R} = \left( \frac{F}{2\pi\sqrt{Y_{eff}\kappa}} \right) \left| \frac{\theta}{\sin(2\theta)} \right|. \quad (26)$$

The slope is determined by the pressure dependent phase angle. For low dimensionless pressures,  $\theta/\sin(2\theta)$  is close to  $\pi/4$ , while for high pressures it decreases with pressure as  $\ln(\Pi_0)/\Pi_0$ . The characteristic dimension for the applied force is  $\sqrt{Y_{eff}\kappa}$  (in the nano-Newton range). In the linear response regime, force-deformation curves thus can only measure the *geometrical mean*  $\sqrt{Y_{eff}\kappa}$  of the effective Young's modulus and the bending modulus.

The full dimple profile equation (25) is shown in Fig. 5. Note that the depth decreases with increasing internal pressure—which is reasonable—and that the characteristic size of the dimple is independent of internal pressure.

The effective Young's modulus of the shell is thus reduced with respect to its bare value by the coupling between elastic and internal degrees of freedom. Note that there is no corresponding reduction of the bending modulus. If the curvature of the Gibbs free energy is sufficiently small, then the effective Young's modulus will become negative at a threshold value  $d^2 g/d\eta^2 = 4\gamma^2/Y$ . The location of this elastic instability can be seen to reduce our earlier requirement  $d^2 g_0/d\eta^2 > \gamma_0^2/K$  for thermodynamic stability using  $\gamma = \gamma_0\mu/(\mu+K)$  and  $Y = 4K\mu/(K+\mu)$ . Elastic instabilities of this type are expected in particular if the curvature  $d^2 g_0/d\eta^2$  is small at the transition point, i.e., if the transition is weakly first order. Softening of the Young's modulus has been observed for the case of the swelling transition of CCMV as discussed in the conclusion. Note that the effective dimple radius diverges as one approaches the elastic instability so the linear response description actually must break down near the transition point. Note also that because of this renormalization of the Young's modulus, the elastic stiffness of

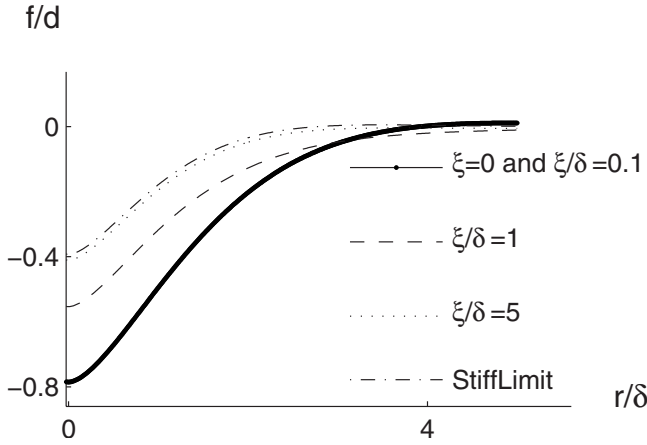


FIG. 6. Numerically computed linear response profiles in the crossover regime where the capsid dimple size  $\delta$  is comparable to the characteristic length scale  $\xi$  for the spatial variation of the reaction coordinate. The ratio of the effective and bare Young's moduli was fixed at  $1/4$ .

the initial and final states in general will be different, which will play an important role in the following section.

### 2. $R \ll \xi^2/l_B$

If one increases the cooperativity, then the healing length  $\xi_{\pm} = \sqrt{\Gamma/g''(\eta_{\pm})}$  can exceed the dimple size  $\delta \sim (Rl_B)^{1/2}$ . In that regime, we now can drop the left-hand side of Eq. (22),

$$\kappa \Delta^2 f - \sigma_0 \Delta f + \frac{Y}{R^2} f \approx -F \delta(\vec{r}). \quad (27)$$

The only difference between Eqs. (27) and (24) is that the effective Young's modulus has been replaced by the bare Young's modulus. Increasing cooperativity thus has the effect of increasing the in-plane elastic stiffness of the capsid.

### 3. $R \sim \xi^2/l_B$

In the crossover regime with  $R \sim \xi^2/l_B$ , one must solve Eq. (22) numerically. The resulting dimple profile is shown in Fig. 6 for different values of the ratio  $\xi/\delta$ . As expected, the indentation at the origin progressively diminishes as one decreases the cooperativity. The profile can be approximated by the solution of Eq. (24) if  $\xi/\delta$  is less than 0.1 and by Eq. (27) if  $\xi/\delta$  exceeds 5.0.

## B. Force-induced phase coexistence

We now turn to the case of a shell in a state of phase coexistence. The linear-response approximation is in general no longer valid because the application of even a weak perturbation can produce large-scale changes, due to displacement of domain boundaries. We will focus on the simple case of a circular phase boundary separating two sections of a capsid that are, respectively, in the contracted and the expanded state. The reaction coordinate varies between the two limiting values  $\eta_+$  and  $\eta_-$  across the boundary and the width of the phase boundary is of the order of the healing lengths

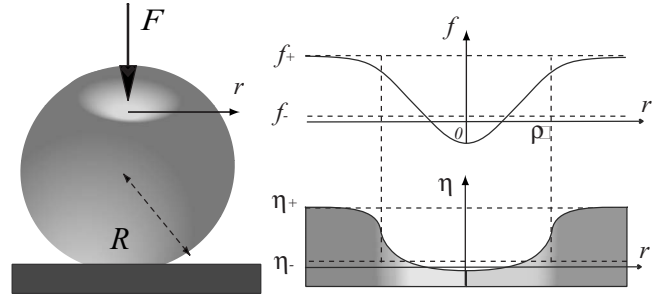


FIG. 7. Phase coexistence induced by a force probe. The capsid is initially in a radially swollen state where  $f=f_+$  and  $\eta=\eta_+$ . The point force produces a circular region of radius  $\rho$  inside of which the capsid is in the contracted state with  $f=f_-$  and  $\eta=\eta_-$ .

$\xi_{\pm} = [\Gamma/g''(\eta_{\pm})]^{1/2}$  for the spatial variation of the reaction coordinate.

For simplicity, we will restrict ourselves here to the regime of large capsids with the healing lengths small compared to the domain radius. That means the radial displacement  $f$  will not vary significantly across the boundary and have a value close to the  $f_b$  of the Maxwell construction of Sec. II. According to Eq. (21), the free energy per unit length of the domain boundary equals

$$\Lambda = \int_{-\infty}^{+\infty} \left( \frac{1}{2} \Gamma \left( \frac{d\eta}{dn} \right)^2 + g_0(\eta) - \frac{2\gamma}{R} f_B \eta \right) dn, \quad (28)$$

which we can interpret as a *line tension*. Here,  $n$  is the normal to the phase boundary. Equation (28) is familiar from studies of the physics of domain boundaries and it can be minimized with respect to the reaction coordinate profile by standard methods of variational calculus. Although the result depends on the specific form of  $g_0(\eta)$ , the line tension is in general of order  $\Lambda \sim \xi \Delta E/a^2$  with  $\Delta E$  the activation free energy barrier per protein—assumed to be in the range of a few  $k_B T$ s—and  $a^2$  the area per protein (of order  $\text{nm}^2$ , see also Fig. 1). The line tension is thus in the range of  $k_B T$  per nm or larger, depending on the magnitude of the healing length.

We will assume that an external point force is applied to a capsid in the swollen state with the circular domain of contracted state surrounding the force, as shown in Fig. 7.

The radius  $\rho$  of the phase boundary must be obtained by minimizing the total capsid free energy,

$$\begin{aligned} \mathcal{F}_T = & \int_{r < \rho} dS \left( \frac{\kappa}{2} (\Delta f)^2 + \frac{\sigma_0}{2} (\vec{\nabla} f)^2 + \frac{Y_-}{2R^2} f^2 + F f \delta(\vec{r}) \right) \\ & + \int_{r > \rho} dS \left( \frac{\kappa}{2} (\Delta f)^2 + \frac{\sigma_0}{2} (\vec{\nabla} f)^2 + \frac{Y_+}{2R^2} (f - f_+)^2 \right) \\ & + 2\pi\rho\Lambda - \pi\rho^2\Delta\mu. \end{aligned} \quad (29)$$

The first two terms represent the deformation elastic energies of sections of the capsid that are far from the domain wall. We use the linear-response approximation for these regions [see Eq. (21)] with  $Y_-$  and  $Y_+$  the effective Young's moduli of, respectively, the swollen and contracted states (recall that these are, in general, different due to the strain renormaliza-

tion discussed in Sec. II). The third term is the free energy cost of the line tension of the circular phase boundary and the last term is due to the difference between the effective free energies per unit area of the two states [see again Eq. (21)],

$$\Delta\mu = \Delta g + \frac{Y}{R^2} f_+^2 - \frac{2\gamma}{R} f_+ \eta_+. \quad (30)$$

If one would neglect the elastic stress contributions, then the radius of the coexistence domain would be simply determined by the condition that the work by the external force had to be of the order of the free energy cost of creating the coexistence domain,

$$F(\rho)\Delta R \sim |\Delta\mu|(\pi\rho^2) + \Lambda(2\pi\rho) \quad (\rho \gg \xi), \quad (31)$$

with  $\Delta R$  the difference between the radii of the two states.

The deformation profiles far from the phase boundary still can be obtained as solutions of the linear-response equation (see Eq. (24)), but they have to be matched at the phase boundary, and we must determine the boundary conditions. According to Eq. (19),  $\Delta^2 f$  must be discontinuous across the

phase boundary—at least on length scales large compared to  $\xi$ —because of the discontinuity of the reaction coordinate across the boundary. The radial displacement  $f$  and its first three derivatives are however continuous provided no external forces or torques are exerted on the phase boundary. The capsid free energy can be expressed in terms of the value of  $f$  at the boundary and its derivatives in the form of a variational expression  $H(\rho)$  for the domain radius  $\rho$ ,

$$H(\rho) = \frac{F}{2} f_{r=0} - \kappa \pi \rho f_+ \left( \frac{d}{dr} \Delta f \right)_{r=\rho} + \sigma_0 \pi \rho f_+ \left( \frac{df}{dr} \right)_{r=\rho} + 2\pi\rho\Lambda - \pi\rho^2\Delta u. \quad (32)$$

It might seem that, apart from these boundary conditions, we also should demand the elastic stress to be continuous across the boundary, i.e.,  $(\vec{\sigma} \cdot \vec{n})_{r=\rho^+} = (\vec{\sigma} \cdot \vec{n})_{r=\rho^-}$ . Continuity of the stress was however *already* imposed when we eliminated the strain using Eq. (18). Note that according to Eq. (18), the strain is discontinuous across the phase boundary.

The appropriate solution of the linear response equations can be expressed as combinations of modified Bessel function with complex arguments

$$f(r) = \begin{cases} \left( \frac{FR}{2\pi\sqrt{Y_- \kappa}} \right) \frac{1}{\sin(2\theta)} \operatorname{Im} K_0 \left( \frac{r}{\delta_-} e^{i\theta} \right) + A_1 \operatorname{Im} I_0 \left( \frac{r}{\delta_-} e^{i\theta} \right) + A_2 \operatorname{Re} I_0 \left( \frac{r}{\delta_-} e^{i\theta} \right), & r < \rho, \\ A_3 \operatorname{Im} K_0 \left( \frac{r}{\delta_+} e^{i\theta} \right) + A_4 \operatorname{Re} K_0 \left( \frac{r}{\delta_+} e^{i\theta} \right) + f_+, & r > \rho. \end{cases} \quad (33)$$

The coefficients  $A_{1-4}$  must be obtained by imposing the four boundary conditions on  $f$  and its derivatives. This procedure was carried out numerically. The result was inserted into the variational energy  $H(\rho)$ , Eq. (33), for the domain wall radius. The plots of Fig. 8 show the two different cases we encountered.

Figure 8(a) shows  $H(\rho)$  for the case that the ratio  $Y^+/Y^-$  of Young's moduli of the swollen and contracted phases equals 5.0 while Fig. 8(b) shows  $H(\rho)$  for the case that this ratio equals 0.5. Both curves have a boundary minimum at  $\rho=0$  with  $H(\rho=0)=0$ , which corresponds to a capsid in the swollen state. This swollen state boundary minimum is always present. In order for phase coexistence to be thermodynamically stable,  $H(\rho)$  thus must have a second minimum at a finite value for  $\rho$  with  $H(\rho)$  less than zero. In the first—but not the second—case such a minimum indeed developed when the applied force  $F$  exceeded a level of about one nN. The appearance of the coexistence state requires the crossing of a free energy barrier according to Fig. 8.

The free energy of this coexistence state still must be compared with that of the uniform contracted state. Figure 9 shows the—numerically computed—phase diagram for the swollen (+) and contracted (−) states for different values of  $\Delta\mu$  and  $F$ . A region of phase coexistence (+/−) indeed ap-

pears in the phase diagram but, as already indicated by Fig. 8, *only* at force levels exceeding a threshold value of the order of one nN. The region of coexistence region terminates in a line of direct first-order transitions between the swollen and contracted states.

In the limit of small forces, the transition line should be determined by the condition that the mechanical work  $F\Delta R$  by the external force should equal the “chemical” work  $-\Delta\mu A$ , with  $\Delta R$  the difference between the radii of the two states and  $A$  the area of the capsid (dotted line in Fig. 9).

Figure 9 shows that thermodynamic quantities characterizing a capsid conformational transition in principle can be measured by a micromechanical probe. Assume for example that the chemical potential difference  $\Delta\mu$  between the two states depends on an external control parameter, such as, for example, the pH level, and that we wanted to measure  $\Delta\mu(\text{pH})$ . For small  $\Delta\mu$ , measurement of the dependence of the critical force for the transition  $F(\text{pH})$  on pH, can be used to obtain  $\Delta\mu(\text{pH})$  from the relation  $F(\text{pH})\Delta R \approx -\Delta\mu(\text{pH})A$ . One can measure  $\Delta\mu(\text{pH})$  also over a wider range. The bending modulus  $\kappa$  and the Young's modulus  $Y$  of a capsid can be measured by a combination of shape analysis and measurement of the force-deformation curve [4]. The full  $\Delta\mu(\text{pH})$  dependence can then be obtained by combining the

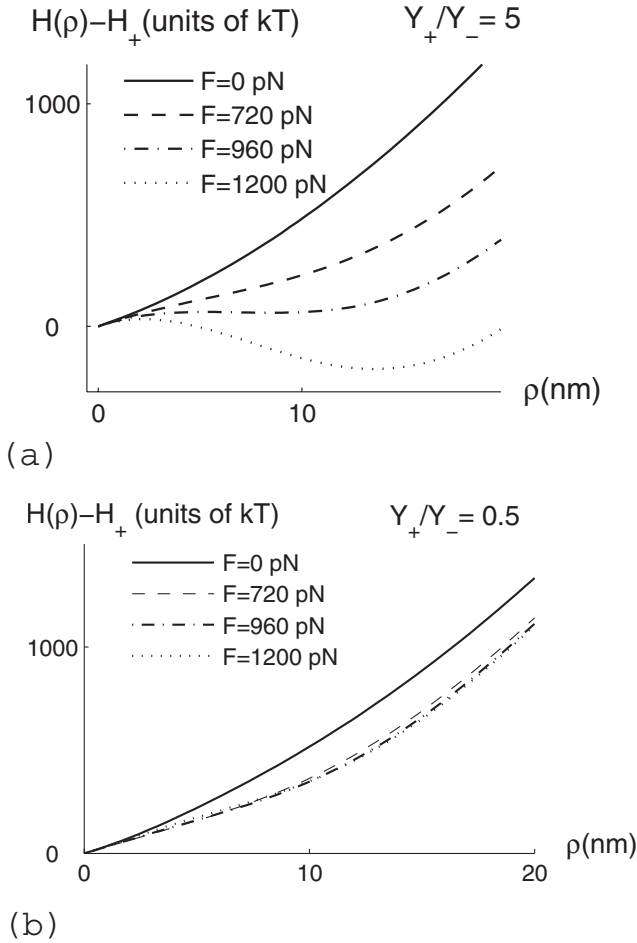


FIG. 8. (a) Numerically computed energy  $H(\rho)$  of a capsid that is in a state of phase coexistence as a function of the radius  $\rho$  of the domain wall. The parameters were  $R=14$  nm;  $\kappa=800$  pN·nm;  $\Delta\mu=-2$  pN/nm;  $\Lambda=20$  pN;  $Y_+=200$  pN/nm, and  $Y_-=40$  pN/nm. The radii of the swollen and contracted state differed by 10%. The horizontal axis is in nm and the vertical axis is in units of  $k_B T$ , with the energy of the initial swollen state subtracted off. Curves 1–4 correspond to force levels  $F$  in the range of 0 to 1.2 nN. A second minimum, indicating phase coexistence, appears for force levels above, approximately, one nanoNewton. (b) Same as (a) except that  $Y_+=200$  pN/nm and  $Y_-=400$  pN/nm. Phase coexistence is not encountered at any force level.

measured  $F(\rho H)$  with the  $\Delta\mu(F)$  curve of Fig. 9 obtained by a numerical solution of Eqs. (7)–(9) for these values of the moduli. The only unknown parameter would be the line tension  $\Lambda$ . However, if the critical force  $F_c$  for the onset of phase coexistence, shown in Fig. 9, can be measured experimentally, then, from the computed dependence of  $F_c$  on  $\Lambda$ , we can find  $\Lambda$ . In conclusion,  $\Delta\mu$  and  $\Lambda$  can be obtained by combining micromechanical measurements with the formalism presented in this paper.

If one compares the two panels of Fig. 8, one sees that elastic stiffness plays an important role in the phase behavior: *if the contracted state has a Young's modulus that is large compared to that of the swollen state, then there is no phase coexistence*. Figure 10 shows the threshold force  $F_{\pm}$  for the onset of phase coexistence at a given  $\Delta\mu$  as a func-

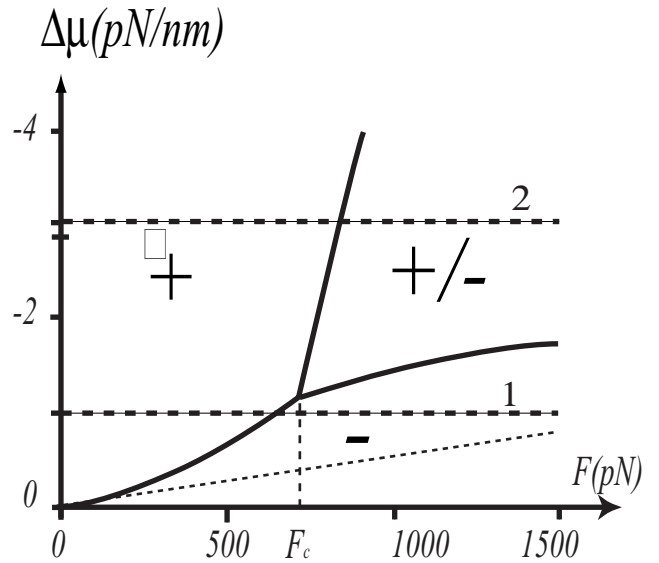


FIG. 9. Phase diagram for the swollen (+), contracted (-), and coexistence (+/-) states of a capsid with  $\Delta\mu$  the free energy difference per unit area between the two states and  $F$  the external point force. Swelling corresponds to a 10% increase of the radius. For lower values of  $\Delta\mu$ , there is a direct transition between the swollen and contracted states (horizontal line marked 1), while for larger values of  $\Delta\mu$  the application of force can produce phase coexistence (horizontal line marked 2) for forces above a threshold  $F_c$ . The dotted line is the linear-response prediction for this transition line. The other parameters were  $\Lambda=2.5$  kT/nm<sup>2</sup>,  $\kappa=100$  kT,  $Y_+=220$  pN nm<sup>-1</sup>,  $Y_-=44$  pN nm<sup>-1</sup>,  $R=14$  nm, and  $\Pi_0=0$ .

tion of the ratio  $Y_+/Y_-$  of the two Young's moduli. The different curves are for different values of the so-called ‘‘Föppl–Von Karman's number’’ (FVK)  $\gamma_{FVK} \equiv YR^2/\kappa$  with  $Y$  the bare Young's modulus, the dimensionless ratio of stretching and bending energies. Internal pressure lowers the threshold force: an internal pressure of ten atmospheres lowers the critical forces by a factor of 2.

The physical reason that phase coexistence depends so sensitively on the stiffness ratio  $Y_+/Y_-$  can be seen from the linear response theory by noting that the work  $f(R=0)F$  by the external force  $F$  is of order  $-F^2R/\sqrt{Y_{\pm}\kappa}$  according to Eq. (26), depending on whether the dimple is in the expanded or contracted state. If the contracted state is softer than the swollen state, then the elastic energy of the system can be reduced by transforming the dimple from the swollen to the contracted state. In the opposite case, this would only increase the elastic energy. The elastic energy thus favors phase coexistence *only* if the contracted state has a Young's modulus that is smaller than that of the swollen state. This mechanism is closely related to the familiar ‘‘stress-induced decomposition’’ [21] of bulk structural phase transitions.

But can one actually tell, by a micromechanical study, whether the capsid is in a state of phase coexistence? In Fig. 11, we show two—numerically computed—force deformation curves (in dimensionless units).

The curve labeled 1 corresponds to the horizontal line  $\Delta\mu=-1$  pN/nm in Fig. 9 with a direct transition at a force level below  $F_c$ . At the transition point, the indentation level  $f(0)$  changes discontinuously. Note (i) that the discontinuity

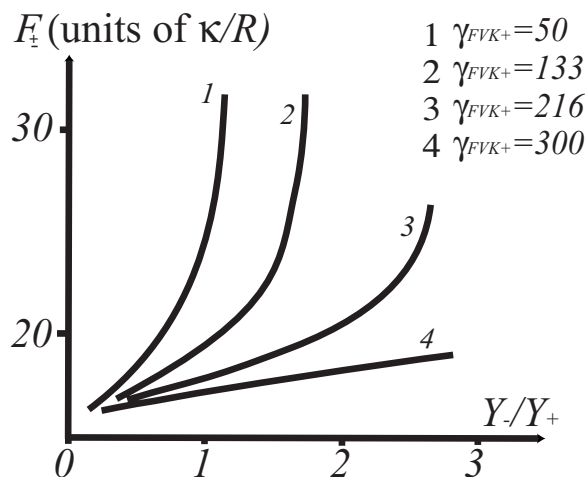


FIG. 10. Threshold force  $F_{\pm}$ , at given  $\Delta\mu$ , for the onset of force-induced phase coexistence as a function of the ratio  $Y_+/Y_-$  of Young's moduli of the swollen, respectively, contracted state for different values of the Föppl-Von Karman number  $\gamma_{FVK+}=YR^2/\kappa$  with  $Y$  the bare Young's modulus. The threshold force is expressed in dimensionless units with  $\kappa$  the bending modulus and  $R$  the capsid radius. The critical force diverges at a threshold that depends on the value of  $\gamma_{FVK+}$ . The remaining parameters are  $\Lambda=0.7kT/\text{nm}$ ,  $\Delta\mu=0.5kT/\text{nm}^2$ ,  $\Pi_0=0$ ,  $\Delta R/R=0.1$ ,  $\kappa=100kT$  and  $R=14\text{ nm}$ .

is larger than the 10% change in radius of the zero force swelling transition and (ii) that the force deformation curves of the swollen (+) and contracted (-) branches are linear. The transition line corresponds to the point where the free energies of the swollen and contracted states are equal. Since both states are locally stable and separated by a substantial energy barrier, estimated to be in the range of hundreds of  $k_B T$ , it is likely that the transition is highly hysteretic.

The curve labeled 2 corresponds to the horizontal line  $\Delta\mu=-3\text{ pN/nm}$  in Fig. 9 that passes through the coexistence region at a force level above  $F_c$ . The bottom section is the linear force-deformation curve of the swollen state. The vertical dotted line corresponds to the transition between the swollen state (+) and the phase-coexistence state (+/-). The discontinuity of the indentation at the transition point is significantly reduced. The key point is that the force-deformation curve of the coexistence state is *strongly nonlinear*. The nonlinearity reflects the motion of the domain wall when the external force is changed. Nonlinear response is in fact a general characteristic of systems in a state of phase coexistence. As a separate experimental check of the theory, it could also be verified that coexistence only is observed if the stiffness ratio  $Y_+/Y_-$  is larger than one. At lower force levels, the coexistence state becomes locally unstable (see Fig. 8) and a spinodal transition to the swollen state must take place. Note, from Fig. 8, that the free energy barrier separating the two states is expected to be tens of  $k_B T$ .

#### IV. CONCLUSION

In this concluding section, we will discuss two well-studied examples of conformational transitions of viral shells in the light of the formalism presented in the preceding sections.

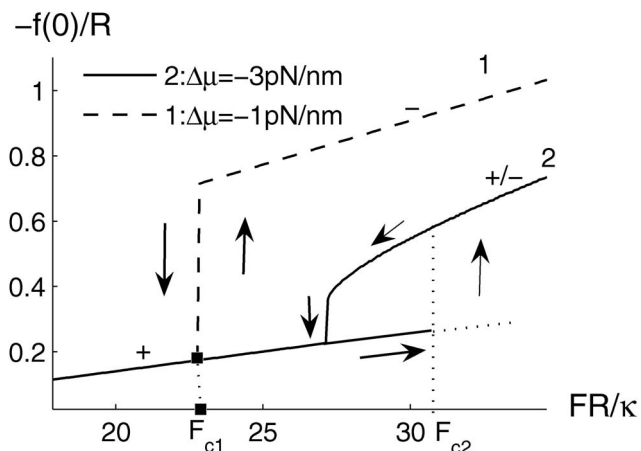


FIG. 11. Force-deformation curves corresponding to the two horizontal lines marked “1” and “2” in Fig. 9. Along curve 1, the capsid is in the contracted state (-) at higher force levels. The vertical dotted line marks a large, first-order transition to the expanded state (+). At  $F_{c1}$ , the contracted and expanded states have the same free energy. Both force-deformation curves are linear. Along curve 2, the capsid is in a state of phase coexistence (marked +/-) at higher force levels. The force-deformation curve is nonlinear. At  $F_{c2}$ , the free energies of the expanded state and the coexistence state are equal.

The *Cowpea chlorotic mottle virus* (CCMV) is a 14-nm radius  $T=3$  spherical plant. Experiments by Jacrot [22] found pronounced hysteresis of CCMV in the titration curves, suggesting a first-order transition between two conformational states of the proteins. X-ray structural studies found [8] that the shell swells by roughly 10% when the pH is raised from 5 to 7 at low ionic strengths. The swelling is accompanied by a protein conformational change that involves a rotation of the capsomers. Removal of  $\text{Ca}^{++}$  ions from the solution has a similar effect. This form of pH driven maturation is in general not irreversible.

The pH level is known to be, in general, an important parameter for the self-assembly of viral shells. The structural integrity of a viral shell is largely determined by the competition between hydrophobic attraction and electrostatic repulsion between subunits, but these generic interactions are not particularly sensitive to the pH level. The pH sensitivity of viral capsids, such as CCMV, is related to contacts between certain very specific pairs of amino acids of subunits, such as Glu and Asp, known as “Caspar pairs” [23]. These Caspar pairs can determine the stability of a capsid when hydrophobic and electrostatic interactions are in balance with each other. As isolated units, the residues have a pK for proton dissociation around 2–4, far outside the physiological range. If, however, only one of a pair loses its proton, then this pair can form a hydrogen bond that dissociates in the physiological range around pK 7. A Caspar pair is stabilized by the presence of  $\text{Ca}^{++}$  ions. Tama and Brooks [13] carried out a normal mode analysis of CCMV and found that the displacement along one privileged single low-energy normal mode had an overlap of more than 95% with the displacement observed during the swelling of the capsid by the x-ray studies. This mode is characterized by a radial expansion, a small

rotation ( $4-6^\circ$ ) of the proteins, and a loss of interaction at the threefold axis of the icosahedral shell, and is indeed driven by dissociation of Caspar pairs.

The association-dissociation reaction of a distribution of Caspar pairs can be described by an Ising model degree of freedom, for example, with “spin up” the bonded state and “spin down” the dissociated state. In the continuum limit, the effective free energy of an Ising model order parameter is precisely of the form proposed in Sec. II. The reaction free energy  $g_0(\eta)$  could thus, at least in principle, be determined from the normal mode calculation. Note that even if two different viral shells have a similar  $g_0(\eta)$ , as is expected to be true for CCMV and CMV shells (which have similar normal mode spectra [13]), then that does not mean that these shells will have the same transition thermodynamics. Because of the coupling to the elastic degrees of freedom of the shell, thermodynamic parameters such as  $\Delta\mu$  will be different.

A key prediction of our formalism is the dependence of the Young’s modulus [Eq. (23)] on the internal degrees of freedom. According to Tama and Brooks, removal of  $\text{Ca}^{++}$  ions—and presumably a  $p\text{H}$  increase as well—should cause further softening of the mode. That would be consistent with the assumption that the curvature of the function  $g_0(\eta)$  at the contracted state minimum  $\eta_-$  is reduced. According to Eq. (23), this, in turn, should lead to a pretransitional softening of the Young’s modulus. Recently, precisely such a  $p\text{H}$ -driven softening of the shell elasticity has been observed in AFM experiments on CCMV [4]. The results indicated that the Young’s modulus dropped from about 450 pN/nm at  $p\text{H}=5$  to about 45 pN/nm at  $p\text{H}=6$ . This very pronounced reduction indicates that the swelling transition of CCMV is only weakly first order with low activation energy barriers. The force-deformation curve close to the swelling transition for the contracted capsid is (nearly) linear and nonhysteretic. The prediction of strongly nonlinear, hysteretic force-deformation curves for the swollen capsid close to the transition provides an unambiguous test for the theory.

HK97 is a member of the bacteriophage family that undergoes a sequence of maturation steps [24]. The capsid of HK97 is a quasi-icosahedral  $T=7$  (*laevo*) shell with 420 subunits. We shall focus on the maturation of “prohead II,” which is believed to be triggered by the packaging of DNA (driven by a motor protein imbedded in the shell). The radius of the shell increases from about 28 nm to about 33 nm during the maturation step. The protein conformational change involves rather large rotations (up to  $40^\circ$  for the “A” and “P” protein domains), a refolding of loops and arms of the proteins, and, eventually, the formation of covalent bonds linking the proteins into “chain mail.” As for CCMV, the conformational change of the HK97 proteins leads to a change in shape of the protein: prohead II is approximately spherical, whereas Head II is faceted.

In the context of this paper, the effect of the packaging of DNA on the shell must be described through an increase of the osmotic pressure  $\Pi_0$ . In Sec. II we saw how osmotic pressure indeed can drive a swelling transition of a capsid, either by activation over an energy barrier or by a spinodal instability. Under equilibrium conditions, the required osmotic pressure would be of the order of  $\Delta g/\Delta R$ , with  $\Delta g$  the

zero pressure difference in free energy per unit area of the two states and  $\Delta R$  the change in radius. If we estimate  $\Delta g$  to be in the range of  $10 k_B T$  per  $\text{nm}^2$ , then the corresponding osmotic pressure would be in the range of tens of atmospheres. The osmotic pressure inside a (different) bacteriophage head has been measured [19] and is indeed in that range (it is due mainly to electrostatic self-repulsion [25]). HK97 presents an interesting complication in terms of applying our formalism. Normal mode analysis of HK97 reports that not one but *two* soft modes are involved [14], both having scalar symmetry. One is associated with motion of the pentamers and one with motion of the hexamers. Clearly, a more complete GL theory of the HK97 transition would have to account for the icosahedral symmetry of the shell. Apart from this complication, HK97 also presents us with an interesting opportunity. Lidmar *et al.* [2] showed that shape changes of icosahedral shells from spherelike to faceted are determined by the FVK number  $\gamma_{FVK}=YR^2/\kappa$ . Shape analysis of HK97 leads to a value of about 1480 for the mature state. Faceting appears if the FVK number exceeds a certain critical value (“buckling threshold”) of about  $10^2$ . If one assumes that prohead II has an FVK number below this threshold and head II an FVK number of order 1480, then, from the respective values of the radii, one finds that the Young’s modulus of prohead I should be about seven times less than that of prohead II. If this is indeed the case—and it still must be confirmed by AFM studies—then HK97 would satisfy the key condition for the appearance of phase coexistence: the swollen state is stiffer than the contracted state. Note that for HK97 the “type II” soft-mode mentioned in the Introduction—associated with the icosahedral symmetry—should be expected to appear as well, possibly mixed with the “type-I” soft mode discussed in this paper.

We conclude by briefly discussing the main limitations of our approach. First, we used continuum theory, which includes the molecular structure of the capsid proteins only through the dependence of certain elastic moduli on protein structure. As noted, continuum theory has been able, so far, to account rather well for measured force-deformation curves. For small  $T=3$  shells, such as CCMV, whose diameter is only an order of magnitude larger than that of the constituent proteins, it would be surprising for continuum theory to be quantitatively accurate. A serious limitation, even within continuum theory, is that we assumed the shell to have spherical rather than icosahedral symmetry. A numerical study comparing the force-deformation curve of spherical and icosahedral shells [4] shows that, though they coincide for weak forces, the force-deformation curve of an icosahedral shell is prone to “failure” by inversion of a five-fold site. Finally, as discussed in the paper, the only reason that we were able to arrive at analytical results is that we could neglect the nonlinear terms of the stress tensor for small force level. The validity condition for that approximation is that the indentation of the shell must be small compared to the buckling radius. This is the case if the applied force is small compared to  $8\kappa/R \sim 500$  pN while all our more interesting results, such as the appearance of phase coexistence, involve forces in the nN range. These last two concerns could be addressed by carrying out the program of this paper but using the finite-element numerical analysis of

Ref. [4] to compute the stresses and strains of an icosahedral shell with an internal degree of freedom. Such a study is in progress. Finally, for large applied forces the size of the dimple becomes comparable to the radius of the viral shell, in which case certain geometrical correction factors associated with the curvature of the shell that we neglected would have to be included.

## ACKNOWLEDGMENTS

The authors would like to thank W. Klug, C. Knobler, Pierre Sens, and Martin Castelnovo for helpful discussions. R.B. would like to acknowledge support from the NSF under DMR Grant No. 0404507 and T.G. from the Ecole Polytechnique.

- 
- [1] D. Caspar and A. Klug, *Cold Spring Harbor Symp. Quant. Biol.* **27**, 1 (1962).
- [2] J. Lidmar, L. Mirny, and D. R. Nelson, *Phys. Rev. E* **68**, 051910 (2003).
- [3] J. P. Michel, I. L. Ivanovska, M. M. Gibbons, W. S. Klug, C. M. Knobler, G. J. Wuite, and C. F. Schmidt, *Proc. Natl. Acad. Sci. U.S.A.* **103**, 6184 (2006).
- [4] W. S. Klug, R. F. Bruinsma, J.-P. Michel, C. M. Knobler, I. L. Ivanovska, C. F. Schmidt, and G. J. L. Wuite, *Phys. Rev. Lett.* **97**, 228101 (2006).
- [5] A. C. Steven, J. B. Heymann, N. Cheng, B. L. Trus, and J. F. Conway, *Curr. Opin. Struct. Biol.* **15**, 227 (2005).
- [6] T. Wilk, I. Gross, B. E. Gowen, T. Rutten, F. de Haas, R. Welker, H.-G. Krausslich, P. Boulanger, and S. D. Fuller, *J. Virol.* **75**, 759 (2001).
- [7] R. H. Cheng, V. S. Reddy, N. H. Olson, A. J. Fisher, T. S. Baker, and J. E. Johnson, *Structure (London)* **2**, 271 (1994).
- [8] J. A. Speir, S. Munshi, G. J. Wang, T. S. Baker, and J. E. Johnson, *Structure (London)* **3**, 63 (1995).
- [9] J. Monod, J. P. Changeux, and F. Jacon, *J. Mol. Biol.* **6**, 306 (1963).
- [10] D. E. Koshland, Jr., G. Nemethy, and D. Filmer, *Biochemistry* **5**, 365 (1966).
- [11] D. L. Caspar, *Biophys. J.* **32**, 103 (1980).
- [12] *Structural Phase Transitions*, edited by K. Muller and H. Thomas (Springer, Verlag, 1981), Vols. 1 and 2.
- [13] F. Tama and C. L. Brooks, 3rd, *J. Mol. Biol.* **318**, 733 (2002).
- [14] F. Tama and C. L. Brooks, 3rd, *J. Mol. Biol.* **345**, 299 (2005).
- [15] J.-C. Toledano and P. Toledano, *The Landau Theory of Phase Transitions* (World Scientific, Singapore, 1987).
- [16] M. Widom, J. Lidmar, and D. R. Nelson, *Phys. Rev. E* **76**, 031911 (2007).
- [17] P. Ceres and A. Zlotnick, *Biochemistry* **41**, 11525 (2002).
- [18] The bending energy is zero if  $f$  obeys the equation  $\Delta f + 2f/R^2 = 0$ . Apart from the trivial case  $f=0$ , this equation only has nontrivial solutions that correspond to a uniform translation of the shell.
- [19] A. Evilevitch, J. W. Gober, M. Phillips, C. M. Knobler, and W. M. Gelbart, *Biophys. J.* **88**, 751 (2005).
- [20] Note that the phase angle becomes imaginary if the dimensionless pressure exceeds one.
- [21] J. W. Cahn, General Electric Research Laboratory Report No. 64-RL-(3561 M), 1964 (unpublished).
- [22] B. Jacrot, *J. Mol. Biol.* **95**, 433 (1975).
- [23] D. Caspar, *Adv. Protein Chem.* **18**, 37 (1963).
- [24] W. R. Wikoff, L. Liljas, R. L. Duda, H. Tsuruta, R. W. Hendrix, and J. E. Johnson, *Science* **289**, 2129 (2000); J. F. Conway, W. R. Wikoff, N. Cheng, R. L. Duda, R. W. Hendrix, J. E. Johnson, and A. C. Steven, *ibid.* **292**, 744 (2001).
- [25] J. Kindt, S. Tzlil, A. Ben-Shaul, and W. M. Gelbart, *Proc. Natl. Acad. Sci. U.S.A.* **98**, 13671 (2001).